Chinese Journal of Polymer Science Vol. 34, No. 4, (2016), 420–430

Chinese Journal of Polymer Science
© Chinese Chemical Society
Institute of Chemistry, CAS
Springer-Verlag Berlin Heidelberg 2016

Aggregation Behavior of Cyclic Rod-Coil Diblock Copolymers in Selective Solvents*

Wen-ping Zhang[a], Xiang-hong Wang[b] and Lin-li He[a**]
[a] *Department of Physics, Wenzhou University, Wenzhou 325035, China*
[b] *Wenzhou Vocational & Technical College, Wenzhou 325035, China*

Abstract The aggregation behavior of cyclic rod-coil (RC) diblock copolymers in dilute solutions is investigated through dissipative particle dynamics simulation. By varying the rod length and coil length, cyclic RC copolymers in selective solvents exhibit various morphologies, including spherical micelle, vesicle, bilayer disc, and ribbon bundle structure. Compared with the equivalent linear RC copolymer, only spherical micelle and barrel bundle phase are observed. Rod length is the major factor that controls the liquid-crystalline behavior of RC copolymer systems, while the coil length has a secondary effect on the aggregate morphology. The size of rod bundle varies with the coil length, especially for the end-to-end ribbon bundle and side-by-side barrel bundle, which are assembled by cyclic and linear RC copolymer solutions. This finding indicates that the ribbon bundle or nanofiber-like structure in cyclic RC copolymers can be obtained by controlling the rod length and coil length, and thus the optical and electrical properties of RC copolymer would be further controlled and optimized. Results illustrate that cyclization of a linear RC copolymer induces remarkable differences in the rod arrangement and aggregation behavior, thereby indicating the competition between interfacial energy, rod orientational entropy, coil stretching entropy, and packing constraints.

Keywords: Cyclic rod-coil; Ribbon bundle; Cyclization.

INTRODUCTION

Self-assembly is an efficient method that is widely employed in natural systems to fabricate useful nanostructured materials. Amphiphilic coil-coil block copolymers consisting of solvophobic and solvophilic flexible coil blocks are of fundamental interests[1]. Rod-coil (RC) block copolymers are further complicated by rigid segments (rod blocks)[2–5]. The rod-like segments are either π-conjugated (semiconducting) polymers, polypeptides, or aromatic rods, which allow for various applications in optoelectronics, optical devices, and biological processes[6]. Self-assembly in RC systems is different from that of the classic coil-coil block copolymer, which depends on the chain connectivity constraint and the incompatibility between different blocks. Given the conformational asymmetry between blocks, rods and coils, and the orientational interaction between anisotropic rods, RC block copolymers exhibit more complex phase behavior, including phase separation and liquid crystalline ordering. Based on the functionality of rigid rod blocks, RC block copolymers with various morphologies in bulk, including layered smectic A and smectic C, zigzag, wavy, and perforated lamellae as well as more conventional phases (such as lamellae, cylindrical, and spherical micelles), have attracted considerable

* This work was financially supported by the National Natural Science Foundation of China (No. 21474076), the Natural Science Foundation of Zhejiang (Nos. Z13F20019 and LY15B040005), and the Science and Technology of Wenzhou (No. G20140054).
** Corresponding author: Lin-li He (何林李), E-mail: linlihe@wzu.edu.cn
Received October 7, 2015; Revised November 26, 2015; Accepted November 27, 2015
doi: 10.1007/s10118-016-1763-y

interests[7–14].

Experimental[15–22], theoretical, and simulation[23–27] studies on the aggregate behavior and micellar morphology of amphiphilic RC block copolymers in solutions as well as in melt have been reported recently. Amphiphilic coil-coil block copolymers in selective solvents would form sphere-shaped interfaces to minimize the contact of solvent molecules with solvophobic blocks. However, in RC block copolymer solutions, packing of the rigid blocks at a curved interface creates liquid crystalline defects. Therefore, interfacial energy, liquid crystalline defect energy, coil stretching entropy, and packing constraints are crucial in determining the overall morphology of RC copolymer aggregates and, as well as the molecule packing of inner structure. Tung *et al*. investigated the aggregate behaviors of PF-*b*-PAA copolymer in dilute solutions of dichloromethane (DCM) and methanol, where DCM is the common solvent for both blocks and methanol is selective for PAA coil blocks. Given various coil fractions and solvent quality, various morphologies, including lamellar, spheres, large compound micelles, vesicles, cylinders, and inverted spheres and cylinders were observed[28, 29]. Koh *et al*. observed the unique micelle-to-vesicle transition of $PHIC_{189}$-*b*-$P2VP_{228}$ block copolymer in a rod-selective solvent. The rod-like PHIC blocks wrapped tangentially the surface of the aggregated hydrophilic P2VP cores to form a surface layer a few nanometres thick. The micelle and vesicle structures could be reversibly interchanged by varying the polymer concentration[30]. Theoretically, Lin and coworkers extended the lattice theory to describe the phase behavior of RC diblock copolymers in solution. RC diblock copolymers exhibit lyotropic mesophases with lamellar, cylindrical, and spherical structures when the copolymer concentration is above a critical value[31]. Moreover, the Brownian dynamics was applied to investigate the self-assembly behavior of RC block copolymers in coil selective solvent. At higher interaction between rods, rod blocks tend to align orientationally and pack hexagonally in the core to form a smectic-like disk structure; subsequently, the disk micelle gradually changes to a new string structure, which further splits into some small aggregates until unimers with decreasing the interaction of rod pairs[32]. Sheng *et al*. provided the full morphological phase diagrams for the RC copolymer self-assembly in selective or mixed solvents by using dissipative particle dynamics (DPD) simulation. The diverse morphologies and morphological transitions were induced by varying the rod-block length, copolymer concentration, and solvent content ratio[33, 34].

The properties of nanostructured materials (especially photoelectric) in RC systems are greatly affected by the molecular packing of rod segments, which is closely related to their micellar morphology. Moreover, the material performance can be tailored easily by controlling the relevant parameters influencing the self-assembly process. The experimental, theoretical, and simulation results have also shown that there is a number of parameters (*e.g*., block length, repulsions between block rods and coils, chain architecture, copolymer concentration, and solvent quality) which can control the nanostructures and local rod arrangement of RC copolymer solutions. Predictably, RC block copolymer with various chain architectures, such as linear-, star-, cyclic-, and branched-shape, has diversified aggregate morphologies and optoelectronic applications. The self-assembly phase behavior of RC block copolymers with the special cyclic architecture, which has no chain ends but possesses two junctions in each monomer, would be remarkably different from that of the corresponding linear RC diblocks. Liu *et al.* demonstrated that cyclic-polymers could be successfully synthesized by various experimental methods. Since the cyclic topology with no chain ends exerts stringent restrictions on backbone conformation, the cyclic-polymer could exhibit unique thermal phase transition behavior, which is drastically different from that of linear case[35, 36].

Recently, only a few experimental studies begin to focus on the rigid-flexible cyclic molecule because of the difficulty in synthesis. Such studies include that of Lee *et al.*, who investigated the self-assembly of RC macrocycles in solid and aqueous solutions. In the study, macrocycles in bulk self-organized into 2-D or 3-D ordered structures (rectangular, orthorhombic, tetragonal, and cubic). In selective solvents, the cyclic molecules self-assembled into barrels or cylindrical aggregates with helical tubular structures, which could provide a new strategy for the design of hollow 1-D nanomaterials with biological and electro-optical functions[37, 38]. We previously constructed a theoretical phase diagram for cyclic RC diblock copolymer melts plotted as interaction parameter and rod composition, which was simultaneously compared with that of their linear counterparts with

the same parameters. The degree of polymerization in a monomer was constant. The cyclization of a linear RC diblock copolymer induced remarkable changes in the phase behaviors in terms of the order-disorder transition ($(\chi N)_{ODT}$), assembled morphology, local rod arrangement, and domain spacing size[39]. However, few simulation or theoretical studies have focused on the micellar phase behaviors from cyclic RC block copolymer solutions. In the current work, DPD simulations are performed to systematically explore the micellar morphological transitions of cyclic RC diblock copolymers with varying block length and solvent quality in selective solvents.

SIMULATION METHOD AND MODELS

DPD technique[40] was originally introduced as a method of accessing larger length and time scales in computer simulations, compared with conventional molecular dynamics, and simultaneously retaining the correct hydrodynamic behavior. In DPD method, the 'beads' or particles represent a group of atoms clustered together. The total force acting on a particle i by the particle j contains three parts: conservative force $\vec{F}_{ij}^{C}$, dissipative force $\vec{F}_{ij}^{D}$, and random force $\vec{F}_{ij}^{R}$, which can be written as the sum of three additive forces.

$$\vec{f}_i = \sum_{i \neq j} (\vec{F}_{ij}^{C} + \vec{F}_{ij}^{D} + \vec{F}_{ij}^{R}) \tag{1}$$

$$\vec{F}_{ij}^{C} = a_{ij}\omega(r_{ij})\hat{r}_{ij} \tag{2}$$

$$\vec{F}_{ij}^{D} = -\gamma\omega^2(r_{ij})(\hat{r}_{ij} \cdot \vec{v}_{ij})\hat{r}_{ij} \tag{3}$$

$$\vec{F}_{ij}^{R} = \sigma\omega(r_{ij})\theta_{ij}\hat{r}_{ij} \tag{4}$$

where $\vec{r}_{ij} = \vec{r}_i - \vec{r}_j$, $r_{ij} = |\vec{r}_{ij}|$, $\hat{r}_{ij} = \vec{r}_{ij} / r_{ij}$, and $\vec{v}_{ij} = \vec{v}_i - \vec{v}_j$. The conservative force $\vec{F}_{ij}^{C}$ for nonbonded beads is a soft repulsive force along the intermolecular vector. The parameter a_{ij} is the maximum repulsion between beads i and j. The weight function $\omega(r_{ij})$ is given by $\omega(r_{ij}) = 1 - r_{ij}$ for $r_{ij} < r_c$ and $\omega(r_{ij}) = 0$ for $r_{ij} \geq r_c$, where r_c is the cutoff radius (*i.e.*, $r_c = 1$) indicating the extent of interaction range. Each of the other two forces ($\vec{F}_{ij}^{D}$ and $\vec{F}_{ij}^{R}$) acts effectively as a heat source, which conserves momentum. Here, γ is the friction coefficient and the noise amplitude σ controls the magnitude of the random force. $\theta_{ij}(t)$ is a randomly fluctuating variable with Gaussian statistics: $<\theta_{ij}(t)> = 0$ and $<\theta_{ij}(t)\theta_{kl}(t')> = (\delta_{ik}\delta_{jl} + \delta_{il}\delta_{jk})\,\delta(t-t')$. In addition, the balance between the random and the friction forces provides the thermostat given that $\sigma^2 = 2\gamma k_B T$, where k_B is the Boltzmann's constant and T is the temperature. In the simulation, the cutoff radius, particle mass, and temperature are chosen as the units of distance, mass, and energy, respectively, *i.e.*, $r_c = m = k_B T = 1$. Here, the system reduced density ρ is 5, and the repulsive parameter a_{ij} in Eq. (2) relates to the experimental Flory-Huggins χ-parameter, through $a_{ii}\rho = 75 k_B T$ and $a_{ij} \approx a_{ii} + 1.45\chi_{ij}$ ($\rho = 5$), where a_{ii} is the repulsion parameter between particles of the same type.

Our model system consists of the cyclic RC diblock copolymer and solvent molecules. The flexible coil (C) is modeled as a chain of several DPD particles. Adjacent particles are connected by an extra harmonic spring force, $f_{ij}^{S} = C^{S}(r_{ij} - r_0)$, with equilibrium bond length $r_0 = (2/3)r_c$ and spring constant $C^{S} = 4$. The rod blocks (R) are modeled by DPD beads arranged in a straight line with a fixed distance D_{b-b} in our simulation. The standard SHAKE routine is used to keep the two end particles of the rod at a fixed distance[14, 41]. Solvent molecules (S) are represented by individual DPD beads. Here, c–R_mC_n and l–R_mC_n are used to represent the cyclic and linear RC diblock copolymer, respectively. The rod length L_r corresponds to $(m-1) \times D_{b-b}$, as a function of m. To unify the expression of the block length, we use the DPD particle number m and n to characterize the rod length L_r and coil length L_c, respectively. The values of a_{ij} among the three different species of DPD beads (C, R, and S) are given by $a_{cc} = a_{rr} = a_{ss} = 15$ and $a_{rc} = 45$, $a_{rs} = 15$. The interactions a_{cs} between coil blocks and solvents are variable, ranging from 15 to 75, suggesting the varied solvent conditions. In this study, we focus on the dilute solutions of cyclic RC copolymers with the polymer concentration $\varphi = 0.1$. Our

simulations are performed in a cubic box of constant volume $V = 25 \times 25 \times 25$, containing 78125 DPD beads for the density $\rho = 5$. Periodic boundary conditions are applied in all directions. The dynamics of the DPD particles are followed by solving the Newton's equation of motion, by means of a modified velocity-verlet algorithm[42] with time steps of $\Delta t = 0.04$ and $\lambda = 0.5$. A typical simulation required 1.0×10^6 steps (corresponding to about 1 μs for typical physical values of the parameters) and the first 0.8×10^6 steps are for equilibrium.

RESULTS AND DISCUSSION

We mainly focus on the aggregate behaviors of a dilute c–R_mC_n solutions with the concentration of $\varphi = 0.1$. First, we display the phase diagram and morphology to illustrate the effects of rod length L_r and coil length L_c on the self-assembly of c–R_mC_n in coil-selective solvent ($a_{rs} = 45$ and $a_{cs} = 15$). The results are compared to those of the equivalent linear RC counterpart. Second, the influence of solvent quality on the aggregate morphologies is presented by the phase diagram of c–R_mC_n solutions with rod length L_r and interaction parameter a_{cs}. The solvent quality is controlled by a_{cs}, which varied from 20 to 75, suggesting the solvent type transited from coil-selective to neutral to rod-selective case, where $a_{rs} = 45$ remains unchanged.

Effect of Rod Length and Coil Length

We first investigate the self-assembly of c–R_mC_n in coil-selective solvent. The phase diagram is constructed in L_r versus L_c, as shown in Fig. 1(a). Four distinct types of aggregate from c–R_mC_n solutions are observed, including spherical micelle, bilayer disc, ribbon bundle, and spherical vesicle structures, which are shown explicitly in Figs. 2(a1–d1) and 2(a2–d2). The lines in Fig. 1 represent the estimated thermodynamic phase boundaries. When the rod length $L_r > 8$, the liquid-crystalline ribbon bundle structure occupies dominantly the phase regions. When $L_r \leq 8$, the aggregated behaviors of c–R_mC_n solutions basically depend on the length ratio of L_r/L_c: spherical micelles are formed for $L_r/L_c < 1$; bilayer discs exist in the phase regions of $L_r/L_c \approx 1$, while vesicles appear with $L_r/L_c > 1$. Especially, the growth and stability of the bilayer disc phase is governed strictly by the length match between rod and coil blocks, which is evidenced by the narrow phase region of disc structure shown in Fig. 1(a). Once the match is imbalanced, the disc structure would be replaced by spherical micelles or hollow vesicles. In other words, the rod length is the major factor controlling the liquid-crystalline behavior of RC copolymer systems, while coil length seems to have a secondary effect on the aggregate morphology.

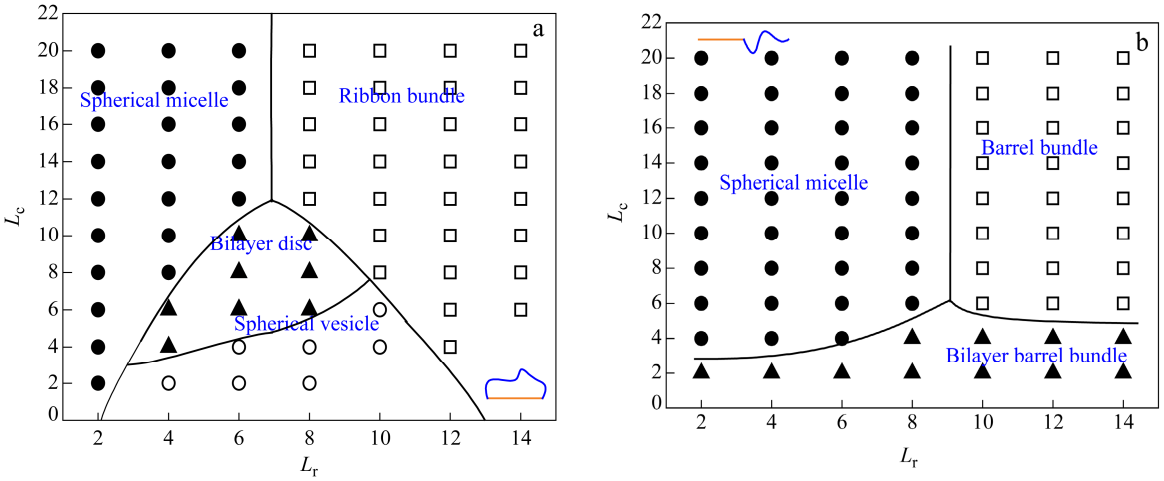


Fig. 1 Phase diagrams of RC copolymer in coil-selective solvent as a function of rod length, L_r, and coil length, L_c, at polymer concentration $\varphi = 0.1$: (a) c–R_mC_n and (b) l–R_mC_n

To illustrate the effect of the coil grafting architecture on the self-assembly behavior of the RC molecule, we also present the phase diagram of l–R_mC_n solutions for comparison (Fig. 1b). Correspondingly, linear RC copolymers self-assemble into spherical micelle, barrel bundle, and bilayer barrel bundle phase. Obviously, the

stable morphologies for the cyclic-shaped RC copolymers are quite different from those of linear counterparts. The difference has been observed partly by our previous studies on the comparison between cyclic and linear RC melts[39]. The internal structure and rod arrangement within diverse aggregates will subsequently be discussed in detail.

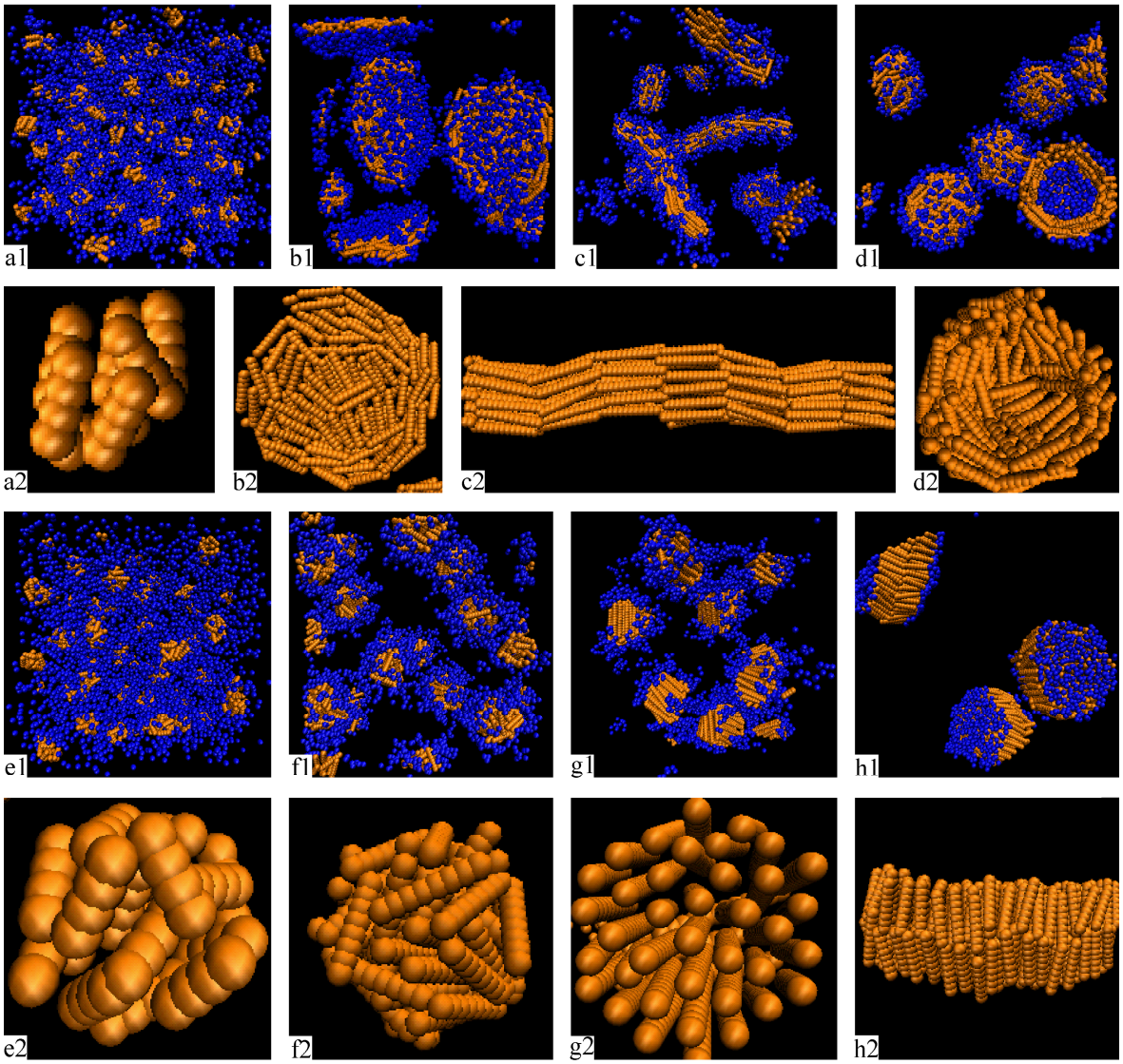


Fig. 2 Morphological snapshots for c–R_mC_n : (a1) spherical micelle with L_c = 8 and L_r = 4, (b1) bilayer disc with L_c = 8 and L_r = 8, (c1) ribbon bundle with L_c = 8 and L_r = 12, (d1) spherical vesicle with L_c = 4 and L_r = 8; for l–R_mC_n: (e1 and f1) spherical micelle, (g1) monolayer barrel bundle and (h1) bilayer barrel bundle (The rod aggregates have been extracted from the simulation cell for viewing ease in (a2–d2) and (e2–h2).)

Figure 2 presents the typical morphologies and only rod aggregates for c–R_mC_n and l–R_mC_n solutions with the same parameters. Generally, with short rods of L_r = 4 and L_c = 8, *i.e.*, $L_r/L_c < 1$, as shown in Figs. 2(a1) and 2(e1), the overall spherical micelles with a coil-corona are observed for RC copolymers regardless of molecular architecture[6], depending primarily on the composition of the incompatible blocks. From the detailed comparison on rod arrangement shown in Figs. 2(a2) and 2(e2), we can see that the rigid rods are packed mostly in orientational order into the core of c–R_mC_n spherical micelles, whereas the rods are arranged radially in the

core of *l*–R_mC_n case. As the rod length is increased to L_r = 8, *i.e.*, $L_r/L_c \approx 1$, a bilayer disc with planar interface is developed for cyclic RC Figs. 2(b1) and 2(b2), while the aggregate remains spherical micelle in linear case Figs. 2(f1) and 2f2. When L_r = 12, *i.e.*, L_r > 8, the orientational interaction between anisotropic rods predominates the aggregation process. For *c*–R_mC_n, the rods are packed end-to-end (Figs. 2c1 and 2c2), presenting the nanofiber structure and inducing the formation of ribbon bundle phase. For the equivalent *l*–R_mC_n, barrel bundle structures, instead of micelles, are formed, where the rods are arranged side-by-side into interdigital barrel bundle (Figs. 2g1 and 2g2). Finally, for L_r = 8 and L_c = 4 case, *i.e.*, $L_r/L_c > 1$, a spherical vesicle is observed for *c*–R_mC_n (Fig. 2d1), and a bilayer barrel bundle phase appears for *l*–R_mC_n case (Fig. 2h1). As illustrated in Figs. 2(d2) and 2(h2), the rods wrap tangentially the spherical cores consisted of the solvophilic coils in the former[30], whereas the rods are arranged neatly into a bilayer smectic A-like phase in the latter. Obviously, the architecture difference in RC molecule remarkably influences the self-assembly of aggregates. For cyclic RC copolymers, the rod is tethered by the coil with two junctions between rod and coil blocks, thus restricting the free degree of rod orientation and seriously influencing the aggregate behavior[39]. This finding is analogous to the study of Ouarti *et al*. on coil-coil copolymer solubilized in selective solvent. They observed that the linear PS-PI copolymers yielded spherical micelles, whereas wormlike cylindrical micelles are formed in cyclic counterparts[43]. Similarly, there are some solvent-induced self-assembly structures of RC observed by the experiment studies. Zheng *et al*., synthesized the new amide macrocycles based on tetraphenylethylene (TPE), and thin or big nanoribbons were formed, which would further self-assembled into microtubes or hollow microspheres depending on the solvent conditions[44]. Lee *et al*., also presented the self-assembly of macrocyclic amphiphiles in water from spheres, helical coils to vesicles with an increase in the molecular length of the macrocycle[45]. Correspondingly, for the case of linear RC, Wan *et al*., reported that the solvent-induced different aggregation behaviors of PEO104-*b*-PMBPS53. In dioxane/water, spherical micelles were confirmed by TEM, whereas barrel-like structures were formed in THF/water, where PEO104-*b*-PMBPS53 formed liquid-crystalline domains in the cores of micelles with PMBPS oriented parallel[46].

Comparing the two phase diagrams shown in Fig. 1, we can find that the liquid-crystalline phase (ribbon or barrel bundle) covers dominantly the phase regions with L_r > 8, which is in agreement with the studies of Sheng *et al*. on RC copolymer dilute solutions. In their linear RC systems with rod length L_r > 8, the neighboring rods begin to align with each other and exhibit the liquid-crystalline ordering[33, 34]. The theoretical works of Chen *et al*. have pointed out that, for RC systems, the stable phase structure depends on the competition between enthalpy and entropy within systems[13]. Rods attempt to align orientationally to maximize their contact and minimize interfacial energy, while coils attempt to maximize free volume to maximize entropy. The competition results not only directly determine the fashion of rod orientational packing and coil free stretching, but also influence the overall morphology of RC solutions. Then, take L_r = 12 and L_c = 8–20 for example, shown in Figs. 3 and 4, *c*–R_mC_n and *l*–R_mC_n solutions separately assemble into ribbon and barrel bundle phases, where the packing fashions of the rods are significantly different. This variation can be reasonably well explained by the different coil grafting architectures. When a coil block is grafted to the one end of a rod, *i.e.*, linear RC diblocks, the rods in the aggregate structures take interdigitated[5] or chiral[19] packing fashion to reduce the elastic stretching energy of the coils. When a coil block is grafted to the two ends of a rod, *i.e.*, cyclic RC diblocks, the copolymers can only take loop conformation, where the rods are connected end-to-end into the worm-like or ribbon-like phase to maximize the orientational entropy between anisotropic rods.

From Figs. 3 and 4, we also can see that the long rods dominate the aggregate process, governing the self-assembled morphologies and rod packing fashions, *i.e.*, *c*–R_mC_n and *l*–R_mC_n solutions each maintain ribbon and barrel bundle phases with the increase of coil length L_c. However, the coils seem to have a secondary effect, *i.e.*, the number and size of bundle aggregates varies as L_c. With L_c increased from 8 to 20, shown in Figs. 3 and 4, the number of aggregates increases, and the size of each rod aggregate becomes small. To make the above observations quantitatively, Fig. 5 displays the average size of rod aggregates along the longitudinal section of a ribbon bundle ($< N_{cyclic} >$) or the lateral section of a barrel bundle ($< N_{linear} >$) as a function of L_c for L_r = 10 and 12, respectively. Apparently, the value of $< N_{cyclic} >$ or $< N_{linear} >$ decreases as L_c increases for both linear and

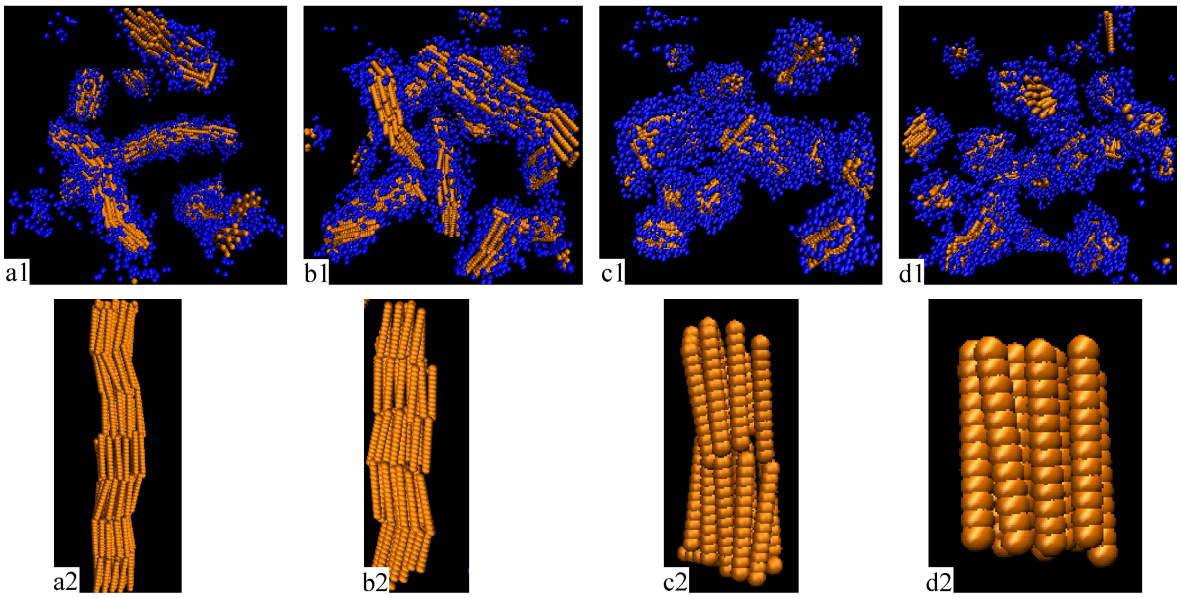


Fig. 3 Ribbon bundle phases of c–R_mC_n solutions with L_r = 12 and L_c = 8, 12, 16 and 20 (a1–d1) (For viewing ease, just rod aggregates are shown in a2–d2.)

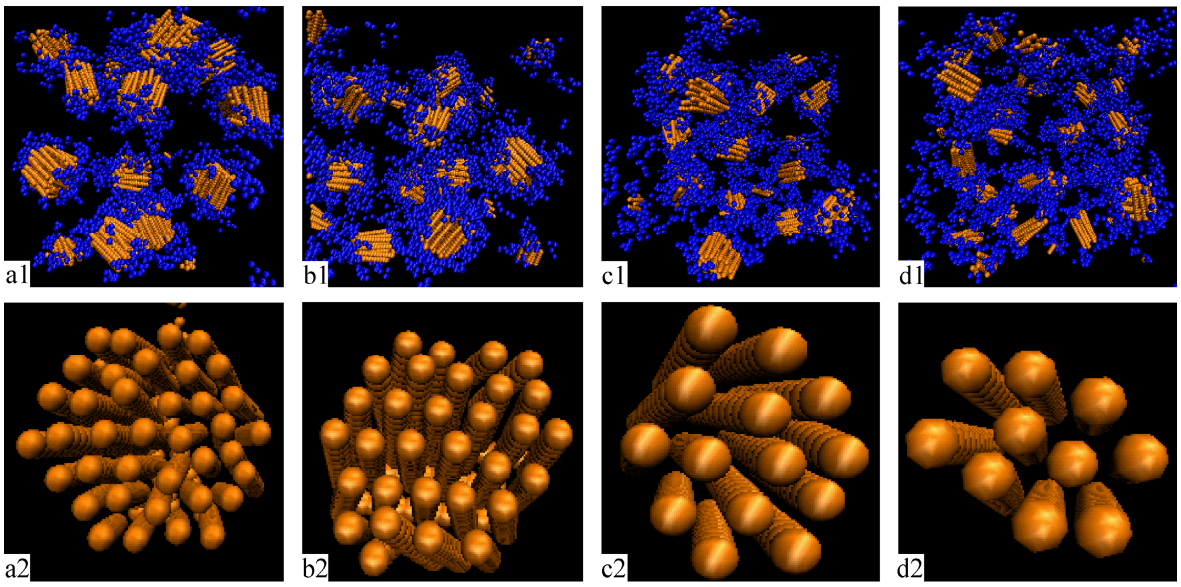


Fig. 4 Barrel bundle phases of l–R_mC_n solutions with L_r = 12 and L_c = 8, 12, 16 and 20 (a1–d1) (Just rod aggregates are shown in a2–d2.)

cyclic RC copolymers. The growth and stability of bundle structures are controlled by the orientation of the solvophobic rod blocks, therefore once the orientation is formed, more copolymers will join in, attempting to cover the solvophilic edge of the bundle. However, large bundle aggregates would split into many independent bundles when L_c increases to a certain value. This finding results from the attempt of long coils to maximize their free volume to maximize entropy and RC packing frustration. Consistent with the RC case, for the conventional coil-coil copolymers in diluted solutions, the mean size of a single aggregate also decreases with increasing soluble-block length[47]. Therefore, cyclic RC systems can be self-assembled into ribbon bundles or nanofibers by controlling the disturbance from the elastic energy of coils. The highly-ordered structure of

ribbons or so-called nanofibers exhibits a considerable potential in conductivity and electronically conductive groups[48]. Furthermore, these nanofiber-like phases are of particular interest for optical and electronic properties and widely used in the area of light-emitting diodes, optical and electronic devices, and so on[49, 50].

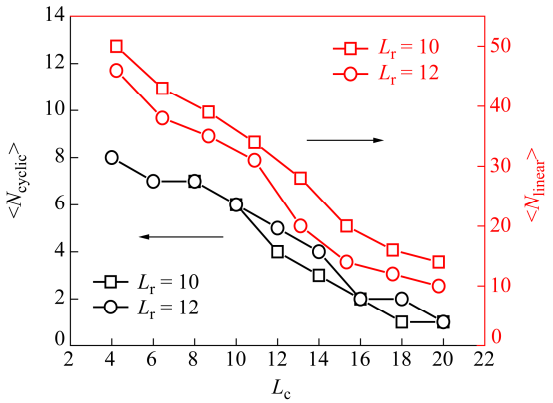


Fig. 5 Average size of rod aggregates along longitudinal section of a ribbon bundle ($< N_{cyclic} >$) or lateral section of a barrel bundle ($< N_{linear} >$) as a function of L_c

Effect of Interactions between Coil and Solvent

The micellar morphologies of cyclic RC copolymer in solutions are significantly affected by the solvent conditions[33, 34]. The solvent quality represents the degree of selectivity to either block, which is controlled by the interactions a_{cs} and a_{rs} in our simulation. In this study, we fix $L_c = 8$ and $a_{rs} = 45$ with varying L_r from 2 to 14 and a_{cs} from 20 to 75, where a_{cs} controls the solvent type to transit from coil-selective to neutral to rod-selective case. The phase diagram and diverse morphologies are shown in Fig. 6. As the rod block is short, such as $L_r = 2$, the orientational driving force between rods is weak. Consequently, the rods that formed small aggregates are dispersed within the coil continuous phase domains, forming spherical micelle (SM_r) phase, generally irrespective of the value of a_{cs}. On the contrary, as L_r increases greater than or equal to 10, the driving force from rigid rod becomes stronger; the internal architecture of spherical micelle (SM_c) is built by rod blocks, while coil aggregates are scattered in rod continuous phase domains. Nevertheless, as the repulsive interactions between coil blocks and solvents exceed a certain value, such as a_{cs} = 75, the coil-filled micelle (S'_{crcr}) is wrapped completely by rod blocks. As L_r = 4, the perforated concentric spherical micelle appears in turn from $PS_{rcrc}$to PS_{crcr} with increasing a_{cs}. Furthermore, as L_r = 6–8, the solvent effect on the aggregation behavior of cyclic RC solutions becomes more obvious. Take $L_r = 8$ for example, in coil-selective solvent case, cyclic RC is assembled into concentric spheres with rod core and alternating coil or rod shell (S_{rcrc}), but a reverse phase with coil core (S_{crcr}) appears in rod-selective solvent. When the condition is close to neutral solvent, the lamellar structure (*Lam*) with alternating coil or rod sheets occupies dominantly the phase region.

To further describe the internal structure of various spherical micelles, Fig. 7 displays the density distributions of different components (rod, coil, and solvent) relative to the mass center for some typical spherical aggregates. For short rod case (L_r = 2), only spherical micelles (SM_r) appear regardless of a_{cs}. From Fig. 7(a2), we can see that there are still high amount of coil blocks existed even if the rod density distribution reaches the peaks, and meanwhile, coil block density is always greater than that of rod block. It is further indicated that the rod aggregates are embedded sporadically into coil bodies. However, for L_r = 8 and a_{cs} = 20 shown in Fig. 7(b2), the distributions of rods and coils present peaks and valleys in turn, *i.e.*, the peaks of rods correspond exactly to valleys of coils. The spherical micelles (S_{rcrc}) with rod core and alternating coil or rod shells are formed. In addition, considering the case of a_{cs} = 70, the density distribution in Fig. 7(c2) is just opposite to that in Fig. 7(b2), illustrating that the reverse spherical micelles (S_{crcr}) with coil core are formed in rod-selective solvent. Meanwhile, the radius of core or shell can be read easily from the density profiles shown

in Figs. 7(b2) and 7(c2). In most linear RC copolymer solutions, the selective solvents result in the formation of monolayer micelles or bilayer vesicles, with the more soluble blocks exposed to the solvents[6]. The final nanostructure of RC solutions depends on the competitions between interfacial energy, coil stretching entropy, liquid crystalline defect energies, and packing constraints. In this study, the cyclization of linear RC copolymer also induces remarkable changes on the self-assembled nanostructures considered in different solvent conditions. The diverse morphology includes filled, perforated, and concentric spherical micelles, and even flat lamellae structures.

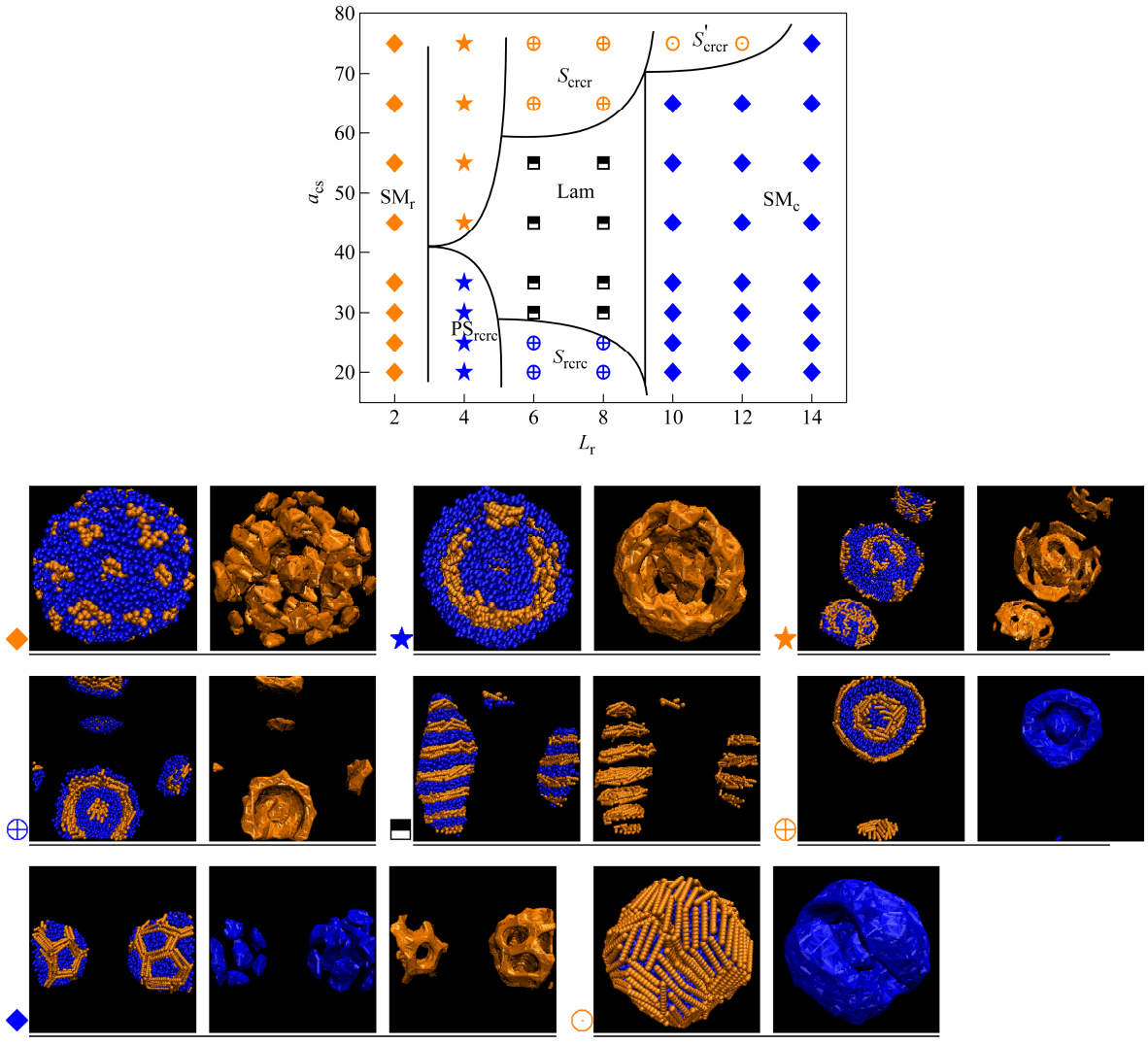


Fig. 6 Phase diagram of c–R_mC_n solutions as a function of rod length, L_r, and solvent interaction, a_{cs} (Here $L_c = 8$ and $a_{rs} = 45$.)

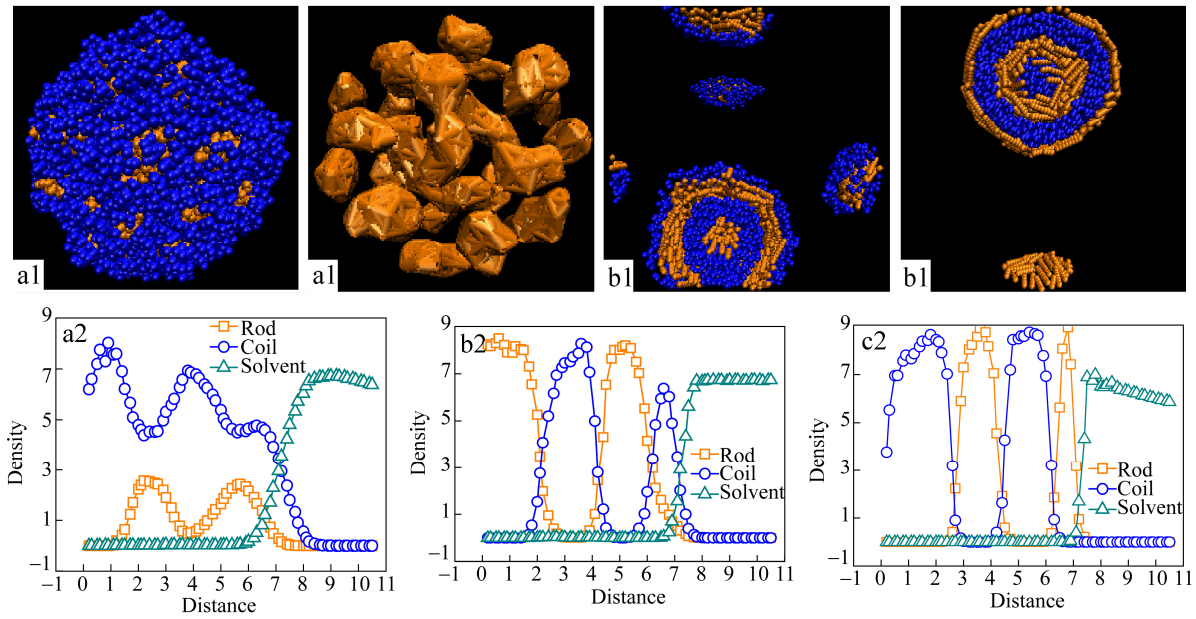


Fig. 7 Morphologies and radial density distributions for (a1, a2) $L_r = 2$, (b1, b2) $L_r = 8$, $a_{cs} = 20$, and (c1, c2) $L_r = 8$, $a_{cs} = 70$

CONCLUSIONS

The solvent-induced aggregation behavior and morphology transition of cyclic RC copolymers in dilute solutions are studied by dissipative particle dynamics simulation. Variations in molecular architecture, rod length, coil length, and solvent quality resulted in different rod arrangements and solution nanostructures.

In coil-selective solvent case, the difference between phase diagrams of cyclic and equivalent linear RC copolymer solutions indicates that the cyclization of RC molecules induces remarkable influence in self-assembled nanostructure. Given that the rods are relatively large for cyclic RC copolymers, orientational interactions between anisotropic rods dominate the formation of ribbon bundle phase or nanofiber-like structure, in which the rods are organized by end-to-end. For comparison in linear case, a barrel bundle phase is observed, in which the rods are arranged chirally in side-by-side. Consequently, the increase in coil length also affects the size of rod aggregate, in which large bundle aggregates would split into independent bundles of rods, thereby accommodating sufficient interfacial area to maintain the bundle structure. Moreover, the solvent quality also affects the aggregation behavior of cyclic RC solutions. Various aggregate morphologies, including filled, perforated, and concentric spherical micelles, as well as flat lamellae structure, are observed when solvent types and rod lengths are varied. By contrast, typical monolayer micelles or bilayer vesicles are formed in linear counterparts.

In conclusion, the interplays between coil stretching entropy, liquid crystalline orientational entropy, interfacial energy, and packing constraints are crucial to the formation of different nanostructures of RC copolymers in solutions. The rich morphologies, especially the nanofiber-like structure of cyclic RC copolymers, provide opportunities for various applications, particularly in electronic and optoelectronic devices.

REFERENCES

1 Hamley, I.W., "The physics of block copolymers", Oxford University Press, Oxford, 1998
2 Chen, J.T., Thomas, E.L., Ober, C.K. and Mao, G.P., Science, 1996, 273: 343
3 Jenekhe, S.A. and Chen, X.L., Science, 1998, 279: 1903
4 Lee, M., Cho, B., Kim, H., Yoon. J. and Zin, W., J. Am. Chem. Soc., 1998, 120: 9168

5 Rubatat, L., Kong, X., Jenekhe, S.A., Ruokolainen, J., Hojeij, M. and Mezzenga, R., Macromolecules, 2008, 41: 1846
6 Olsen, B.D. and Segalman, R.A., Mater. Sci. Eng., R, 2008, 62(2): 37
7 Chen, J.T., Thomas, E.L., Ober, C.K. and Hwang, S.S., Macromolecules, 1995, 28: 1688
8 Radzilowski, L.H., Carragher, B.O. and Stupp, S.I., Macromolecules, 1997, 30: 2110
9 Ryu, J.H., Oh, N.K., Zin, W.C. and Lee, M.J., J. Am. Chem. Soc., 2004, 126, 3551
10 Lee, M., Cho, B.K., Ihn, K.J., Lee, W.K., Oh, N.K. and Zin, W.C., J. Am. Chem. Soc., 2001, 123: 4647
11 Horsch, M.A., Zhang, Z.L. and Glotzer, S.C., Phys. Rev. Lett., 2005, 95: 056105
12 Chen, J.Z., Zhang, C.X., Sun, Z.Y., Zheng, Y.S. and An, L.J., J. Chem. Phys, 2006, 124: 104907
13 Song, W.D., Tang, P., Qiu, F., Yang, Y.L. and Shi, A.C., Soft Matter, 2011, 7: 929
14 AlSunaidi, B.A, den Otter, W.K. and Clarke, J.H.R., Philos. Trans. R. Soc. London, Ser. A, 2004, 362: 1773
15 Jenekhe, S.A. and Chen, X.L., Science, 1999, 283: 372
16 Chochos, C.L., Tsolakis, P.K., Gregoriou, V.G. and Kallitsis, J.K., Macromolecules, 2004, 37: 2502
17 Radzilowski, L.H. and Stupp, S.I., Macromolecules, 1994, 27: 7747
18 Stupp, S.I., LeBonheur, V., Walker, K., Li, L.S., Huggins, K.E., Keser, M. and Amstutz, A., Science, 1997, 276: 384
19 Lee, M., Cho, B.K. and Zin, W.C., Chem. Rev., 2001, 101: 3869
20 Park, J.W. and Thomas, E.L., Macromolecules, 2004, 37: 3532
21 Wu, J., Pearce, E.M., Kwei, T.K., Lefebvre, A.A. and Balsara, N.P., Macromolecules, 2002, 35: 1791
22 Hu, J.M., Zhang, G.Y., Geng, Y.H. and Liu, S.Y., Macromolecules, 2011, 44: 8207
23 Halperin, A., Macromolecules, 1990, 23: 2724
24 Williams, D.R.M. and Fredrickson, G.H., Macromolecules, 1992, 25: 3561
25 Muller, M. and Schick, M., Macromolecules, 1996, 29: 8900
26 Matsen, M.W. and Barrett, C., J. Chem. Phys., 1998, 109: 4108
27 Jiang, Y. and Chen, J.Z.Y., Phys. Rev. Lett., 2013, 110: 138305
28 Tung, Y.C., Wu, W.C. and Chen, W.C., Macromol. Rapid Commun., 2006, 27: 1838
29 Lin, C.H., Tung, Y.C., Ruokolainen, J., Mezzenga, R. and Chen, W.C., Macromolecules, 2008, 41: 8759
30 Koh, H.D., Par, J.W., Rahman, M.S., Changez, M. and Lee. J.S., Chem. Commun., 2009, 4824
31 Lin, J.P., Lin, S.L., Zhang, L.S. and Nose, T., J. Chem. Phys., 2009, 130: 094907
32 Lin, S.L., Numasawa, N., Nose, T. and Lin, J.P., Macromolecules, 2007, 40: 1684
33 Chou, S.H., Tsao, H.K. and Sheng, Y.J., J. Chem. Phys., 2011, 134: 034904
34 Chou, S.H., Wu, D.T., Tsao, H.K. and Sheng, Y.J., Soft Matter, 2011, 7: 9119
35 Xu, J., Ye, J. and Liu, S.Y., Macromolecules, 2007, 40: 9103
36 Ge, Z.S., Zhou, Y.M., Xu, J., Liu, H.W., Chen, D.Y. and Liu, S.Y., J. Am. Chem. Soc., 2009, 131: 1628
37 Yang, W.Y., Lee, E. and Lee, M., J. Am. Chem. Soc., 2006, 128: 3484
38 Yang, W.Y., Ahn, J.H., Yoo, Y.S., Oh, N.K. and Lee, M., Nat. Mater., 2005, 4: 399
39 He, L.L., Chen, Z.L., Zhang, R.F., Zhang, L.X. and Jiang, Z.T., J. Chem. Phys., 2013, 138: 094907
40 Hoogerbrugge, P.J. and Koelman, J.M.V.A., Europhys. Lett., 1992, 19: 155
41 AlSunaidi, B.A., den Otter, W.K. and Clarke, J.H.R., J. Chem. Phys., 2009, 130: 124910
42 Groot, R.D., and Warren, P.B., J. Chem. Phys., 1997, 107: 4423
43 Ouarti, N., Viville, P., Lazzaroni, R., Minatti, E., Schappacher, M., Deffieux, A., Putaux, J.L. and Borsali, R., Langmuir, 2005, 21: 9085
44 Song, S., Zheng, H.F., Feng, H.T. and Zheng, Y.S., Chem. Commun., 2014, 50: 15212
45 Kim, J. K., Lee, E., Kim, M.C., Sim, E. and Lee, M., J. Am. Chem. Soc.. 2009, 131: 17768
46 Zhang, J., Lin, W.R., Liu, A.H., Yu, Z.N., Wan, X.H., Liang, D.H. and Zhou, Q.F., Langmuir, 2008, 24: 3780
47 Sheng, Y.J., Wang, T.Y., Chen, W.M. and Tsao, H.K., J. Phys. Chem. B., 2007, 111: 10938
48 Palmer, L.C. and Stupp, S.I., Acc. Chem. Res., 2008, 41: 1674
49 Qian, J.S., Zhang, M., Manners, I. and Winnik, M.A., Trends Biotechnol., 2010, 28: 84
50 Mativetsky, J.M., Kastler, M., Savage, R.C., Gentilini, D., Palma, M., Pisula, W., Müllen, K. and Samorı, P., Adv. Funct. Mater., 2009, 19: 24